Evaluation of the polymorphic forms of ritonavir and lopinavir in raw materials and co-milled systems

Lucas Barboza Moreira Pinheiro [a], Songsheng Tao [c], Elizabeth Culbertson [c], Gabriel Lima Barros de Araujo [e], Simon J.L. Billinge [c,d], Fabio Furlan Ferreira [a,b,*]

[a] Center for Natural and Human Sciences (CCNH), Federal University of ABC (UFABC), Santo André, SP 09210-580, Brazil
[b] Nanomedicine Research Unit (NANOMED), Federal University of ABC (UFABC), Santo André, SP 09210-580, Brazil
[c] Department of Applied Physics and Applied Mathematics, Columbia University, New York, NY, USA
[d] Condensed Matter Physics and Materials Science Department, Brookhaven National Laboratory, Upton, NY, USA
[e] Department of Pharmacy, Faculty of Pharmaceutical Sciences, University of São Paulo, São Paulo, SP, Brazil

ARTICLE INFO

ABSTRACT

Recently, the U.S. Food and Drug Administration (FDA) approved the first oral antiviral drug to treat mild to moderate cases of coronavirus disease. The combination of nirmatrelvir with an already used protease inhibitor class drug, ritonavir, has led to Paxlovid®. Several studies considered drug repositioning as the first trial for new drugs. The precise identification and quantification of polymorphs in raw materials and finished products are important to researchers involved in pharmaceutical development and quality control processes. In this work, we study the solid-state behavior of the antiretroviral drugs ritonavir and lopinavir in raw materials and in milled compositions. The results indicate that mixtures of ritonavir Forms I and II are found in different batches of raw materials from the same manufacturer; besides three equal crystalline samples, an amorphous batch was found in lopinavir. Furthermore, the milling process of the already amorphous lopinavir seems to facilitate the amorphization of ritonavir as well as the production of some unexpected crystalline forms of ritonavir. A phase transition of ritonavir Form I to Form II is only observed when co-milling with amorphous lopinavir. These findings reveal significant variations in phase purity of raw materials that affect the processing and solid-state properties, representing risks for the product quality.

1. Introduction

The human immunodeficiency virus (HIV) is a retrovirus from the *lentivirus genus* that leads to the development of the acquired immune deficiency syndrome (AIDS), characterized by a progressive deterioration of the patient's immunological system (Douek et al., 2009). Due to growing advances in the treatment of HIV in the last decade and its access increase, there has been a 51 % reduction in deaths related to AIDS since its peak in 2004 (UNAIDS, n.d.). In 2020, estimates indicated that approximately 37.7 million people worldwide were living with HIV (UNAIDS, n.d.).

Ritonavir-lopinavir fixed-dose combination, marketed under the trade name KALETRA® (Abbott Laboratories), is a successful tablet co-formulation very important in managing HIV infection (Chandwani and Shuter, 2008). As described below, these antivirals are also considered therapeutic agents for antiviral diseases like coronavirus (COVID-19).

Ritonavir (Fig. 1A) and lopinavir (Fig. 1B), individually, have shown polymorphism with significant implications for their aqueous solubility (Marques, 2017; Parthasaradhi Reddy et al., 2014, 2013). In 1998, several lots of capsules containing an ethanolic solution of ritonavir (Norvir®, Abbot) failed dissolution tests due to the growth of the low-soluble crystalline Form II (Bauer et al., 2001), forcing the manufacturer to reformulate the product. Furthermore, there are reports on the existence of anhydrous forms, hydrates, and solvates (Lemmer and Liebenberg, 2013; Parthasaradhi Reddy et al., 2014), which can also impart solubility regarding lopinavir. Due to the high flexibility of its chemical structure – it has four chiral centers – lopinavir can adopt several molecular conformations, allowing the preparation of both amorphous and crystalline forms (Lemmer and Liebenberg, 2013). To enhance lopinavir bioavailability and pharmacokinetics and reduce its dosage units administered per day, melt extrusion technology was used to produce the co-formulation with ritonavir, bringing several
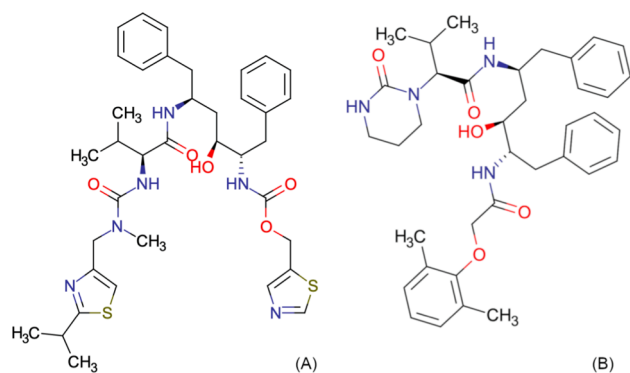

Fig. 1. Ritonavir (A) and lopinavir (B) chemical structures. Blue and red colors represent the nitrogen and oxygen atoms. (For interpretation of the references to colour in this figure legend, the reader is referred to the web version of this article.)

advantages to patients (Klein et al., 2007). The feature crystal arrangement properties, densities, and solubilities of ritonavir are shown in Table 1 and Table 2, and the properties and densities of lopinavir are shown in Table 3.

In March 2020, the World Health Organization (WHO) decreed the SARS-CoV-2 pandemic (severe acute respiratory syndrome) caused by a new coronavirus species. The disease became known as COVID-19, corresponding to COronaVIrus Disease, with its first appearance in December 2019, in Wuhan, Hubei, China. COVID-19 proved highly contagious and is easily spread by contact with secretion on contaminated or vaporized surfaces during clinical procedures, coughing, and even breathing (Prather et al., 2020). Some of those infected need hospitalization and other medical procedures. Following recommendations from the WHO, some potential tests against COVID-19 are underway (Kupferschmidt and Cohen, 2020). Among them, some drugs used to treat malaria and HIV, for example, are being considered. The repositioning of drugs approved by regulatory agencies to treat other diseases can speed up clinical trials. On December 22, 2021, the U.S. Food and Drug Administration (FDA) authorized the first oral antiviral to treat COVID-19. Paxlovid® (Pfizer), which consists of a combination of the antiviral drug nirmatrelvir and ritonavir, is prescribed to treat mild to

Table 1
Crystal arrangement properties, densities, melting temperatures, and melting enthalpies of Forms I and II of ritonavir (Céolin and Rietveld, 2015).

Parameter		Form I		Form II	
Crystal system / Space group		Monoclinic / $P2_1$		Orthorhombic / $P2_12_12_1$	
Melting temperature [°C]		122		125	
Melting enthalpy [J g^{-1}]		78.2		87.8	
Calculated density [g cm^{-3}]		1.2762 (5)[e]	1.325(2)[f]	1.24983 (6)[g]	1.301(1)[h]
Unit cell parameters	a [Å]	13.438 (3)	13.444(2)	10.0236 (3)	9.831(6)
	b [Å]	5.288(1)	5.215(8)	18.6744 (4)	18.485 (11)
	c [Å]	27.055 (5)	26.693(4)	20.4692 (7)	20.261 (12)
	α [°]	90	90	90	90
	β [°]	103.15 (2)	103.456 (2)	90	90
	γ [°]	90	90	90	90
	V [Å^3]	1872.1 (8)	1807(3)	3831.5(2)	3682(4)

Cambridge structural database references:
[e] YIGPIO.
[f] YIGPIO02.
[g] YIGPIO01.
[h] YIGPIO03.

Table 2
Solubility of ritonavir under different concentrations of water/ethanol solutions (Bauer et al., 2001).

Proportion of ethanol/water	Solubility (mg mL^{-1})*	
	Form I	Form II
99/1	90	19
95/5	188	41
90/10	234	60
85/15	294	61
80/20	236	45
75/25	170	30

* Solubility determined at 5 °C.

Table 3
Crystal arrangement properties, densities, melting temperatures, and melting enthalpies of the crystal form lopinavir obtained from methanol recrystallization (L-met) (Marques, 2017).

Parameter		Form L-met[i]
Crystal system / Space group		Triclinic / $P1$
Melting temperature [°C]		95–98
Calculated density [g cm^{-3}]		1.170(5)
Unit cell parameters	a [Å]	11.7101(12)
	b [Å]	14.1111(14)
	c [Å]	24.307(2)
	α [°]	106.314(2)
	β [°]	102.555(2)
	γ [°]	90.570(2)
	V [Å^3]	3751.8(7)

[i] Crystal form of lopinavir obtained from methanol recrystallization.

moderate COVID-19 in individuals > 12 years old, weighing at least 40 kg (Najjar-Debbiny et al., 2022). Further studies must be carried out using *in vitro, in vivo,* and clinical trials for other potential candidates. Thus, a detailed mechanism of the interaction of ritonavir and lopinavir, with different concentrations, is expected.

Due to the importance of the solid-state properties of lopinavir and ritonavir to the dissolution performance of the tablets, several efforts have been undertaken to investigate the amorphous phase and the polymorphism of these drugs. In particular, Kaletra® is produced by amorphous solid dispersion (ASD) technology, which promotes the molecular-scale distribution of both drugs within an amorphous carrier, intending to improve the drugs' dissolution properties (Gurunath et al., 2013; Leuner, 2000). The amorphous phase is important, but it can also affect the production of different polymorphs during processing. For example, it was reported that the desolvation of a crystal-solvent system, theophylline and 2-pyrrolidinone, could be controlled by the type and proportion of polymer used in the polymer-assisted grinding (Terban et al., 2022). Also, the polymorph transformation of a two-component system could be selectively induced by the type of solvent used in the solvent drop-grinding (Trask et al., 2005). Bezzon et al. (Bezzon et al., 2022) have shown the influence of ball milling on the amorphization of flubendazole. The milling process produced a disorder in the mid and long-range orders while maintaining the local structure, thus preventing the fast recrystallization of flubendazole. In the formulation of amorphous solid dispersions of flubendazole loaded in polymeric matrices, Bezzon et al. (Bezzon et al., 2021) have shown that such a composite system prevented the recrystallization of flubendazole, which would improve drug solubility. Ataollahi et al. (Ataollahi et al., 2021) have described how the ball milling processing of efavirenz promoted a gradual transformation of form I to form II in a 2-month window while producing a substantial amorphous contribution after removing the powder from the jars. Erizal et al. (Erizal et al., 2008) inferred that different milling times did not cause a phase transformation in sulfamethoxazole samples; this process only induced defects and a different crystal habit. Descamps et al. (Descamps et al., 2007) have shown that raising the milling temperature above the glass-transition temperature

(T_g) causes a crystal-to-crystal transformation between polymorphic types while lowering the temperature increases the tendency toward amorphization. These findings refute the conventional wisdom that milling changes the physical state only through a heating effect that causes a local melting. Hameed (Hameed, 2019) reviewed how mechanochemistry can be used to induce amorphization, phase transitions, and particle size reduction, which can enhance drug dissolution. The change in polymorphism when grinding the ritonavir and lopinavir mixtures has not been studied yet. For this reason, we have used the co-milling of both drugs in an attempt to verify their amorphization.

In this work, we evaluate the effects of grinding procedures on the polymorphism and amorphous phase behavior of ritonavir and lopinavir mixtures by quantitative phase analysis (QPA) using X-ray powder diffraction data and the Rietveld method and pair distribution function analysis. We found the generation of ritonavir form II on milling in the presence of lopinavir but not when milling pure ritonavir under the same conditions.

2. Materials and methods

2.1. Raw materials

The samples of lopinavir, ritonavir, and KALETRA® were provided by Oswaldo Cruz Foundation (FIOCRUZ), Farmanguinhos unit (Rio de Janeiro, RJ, Brazil). The samples were labeled as presented in Table 4. The manufacturers' names were replaced by the letters A, B, C, D, E, F, G, and H, not to disclose their names. The purity of the samples was inferred by Rietveld refinements using X-ray powder diffraction data, as described in Section 3.1.

2.2. Grinding procedures

Mixtures of ritonavir/lopinavir were prepared at ambient conditions (room temperature, controlled in the laboratory by an air conditioning system – (25 ± 2) °C) by using a ball milling system and an agate mortar and pestle. The samples coded as ball milled (bm) were homogenized in a Retsch MM440 mixer mill system for 30 min at a frequency of 25 Hz, using two 5 mL-steel jars filled with 1-mm-diameter 16 stainless steel balls – these conditions were chosen based on previous experiments; the ones coded as hand-ground (hg) were ground in an agate mortar and pestle for about 20 min. The milled samples were stored in Eppendorf® tubes, stored at room temperature. The description of the samples consisting of physical mixtures between ritonavir and lopinavir, as well as the pure forms, are indicated in Table 5.

2.3. X-ray powder diffraction

X-ray powder diffraction data were collected on a STADI-P diffractometer (Stoe®, Darmstadt, Germany) operating in transmission geometry, using CuK$_{\alpha 1}$ radiation ($\lambda = 1.54056$ Å), with a curved Ge(1 1 1) monochromator. The X-ray photons were detected using a solid-state linear detector (*silicon microstrip*), Mythen 1 K (Dectris®, Baden, Switzerland). The samples were loaded between two cellulose acetate foils. Data were recorded in the range from 2.000° to 112.235° (2θ), with an integration time of 100 s at each 1.05°.

2.4. Optical microscopy

The optical microscopy images were acquired using a Leica DM2700M microscope, equipped with a digital camera with a control software Leica MC120 HD, used to capture and process the images digitally sent by the microscope.

2.5. Differential scanning calorimetry

The DSC measurements were carried out in a TA Instruments DSC-Q200 equipment. The calibration was realized using indium as the reference (156.60 °C, 28.47 J g^{-1}). The samples were weighed and inserted into hermetically sealed crucibles and then inserted into the DSC equipment along with an empty reference crucible. The heating rate was 10 °C min^{-1}, ranging from 25 °C to 150 °C. The weights relative to each sample are shown in Table 5.

2.6. Pair distribution function

The PDF measurements were carried out at the 28-ID-2 beamline of the National Synchrotron Light Source II (NSLS II) at the Brookhaven National Laboratory, NY, USA, using the rapid acquisition PDF method (RA-PDF) (Chupas et al., 2003). A 2D Perkin Elmer amorphous silicon detector was placed 216 mm behind the samples, which were loaded in 1 mm ID Kapton® capillaries and capped with clay. The incident wavelength of the X-rays was $\lambda = 0.1875$ Å. The calibration of the experimental setup was done using nickel as a calibrant. Datasets were collected at room temperature. An inverse frame rate of 0.5 s was used. The total exposure time for each sample was 180 s. The samples used in this method are shown in Table 5, coded as "bm".

Table 5
List of the samples used in all the methods and respective mass fractions (for physical mixtures) – "ar" stands for as-received, "bm" stands for ball-milled, and "hg" stands for hand-ground.

Sample	Description	Mass fraction
L-03 (ar)	Lopinavir 3 (pure form of lopinavir - amorphous)	–
R-04 (bm)	Ritonavir 4 (milled pure Form II of ritonavir)	–
R-06 (bm)	Ritonavir 6 (milled pure Form I of ritonavir)	–
R-06 + L-03 (bm)	Ball-milled physical mixture of L-03 and R-06	79.26 % of L-03 + 20.74 % of R-06
R-06 + L-03 (hg)	Hand-ground physical mixture of L-03 and R-06	79.26 % of L-03 + 20.74 % of R-06
R-04 + L-03 (bm)	Ball-milled physical mixture of L-03 and R-04	84.67 % of L-03 + 15.33 % of R-04
R-04 + L-03 (hg)	Hand-ground physical mixture of L-03 and R-04	84.67 % of L-03 + 15.33 % of R-04
K1 (bm)	Ball-milled commercial sample Kaletra®	–

Table 4
Identification of ritonavir (R), lopinavir (L), and Kaletra® (K) samples according to lot and manufacturer identifications.

ID	Lot	Manufacturer	ID	Lot	Manufacturer	ID	Lot	Manufacturer
R-01	Lot 01	A	L-01	Lot 01	F	K-01	Lot 01	Abbvie®
R-02	Lot 02	A	L-02	Lot 02	F	K-02	Lot 02	Abbvie®
R-03	Lot 01	B	L-03	Lot 03	F			
R-04	Lot 01	C	L-04	Lot 01	G			
R-05	Lot 02	C						
R-06	Lot 03	A						
R-07	Lot 01	A						
R-08	Lot 01	D						
R-09	Lot 01	E						

Data were reduced using a home-written program, *XPDtools,* which is a data analysis pipeline that includes integration with background subtraction between two images, polarization correction, and image-dependent auto masking built on a manual mask background. Corrections were then made to the data, and normalizations were carried out to obtain the total scattering structure function, *F(Q)*, which was Fourier transformed to obtain the PDF using PDFgetX3 (Juhás et al., 2013) within xPDFsuite (Yang et al., 2014). The maximum range of data used in the Fourier transform (Q_{max}, where $Q = 4\pi sin\theta/\lambda$ is the magnitude of the momentum transfer on scattering) was set at 15 Å^{-1} for each of the compounds. A Q_{min} of 0.4 Å^{-1} was used in the Fourier transform due to the beam-stop obscuring the very small-angle scattering.

3. Characterization and quantification of the polymorphs

3.1. X-ray powder diffraction

We carried out a search for the crystallographic information framework (CIF) files of the polymorphic forms of ritonavir in the Cambridge Structural Database System (CSDS) (Groom et al., 2016) and, after that, we performed a qualitative analysis – by visually comparing the peak positions of the experimental diffractograms of each sample with those calculated using the Mercury software (Bruno et al., 2002) – as seen in Fig. 2. It may be clearly noticed the presence of Form I in the samples R-01, R-02, R-06, R-07, R-08, and R-09 and Form II in the samples R-02, R-03, R-04, and R-05, besides the possible presence of characteristic peaks of Form II of very low intensity in the samples R-01, R-07, and R-09.

A similar analysis was performed on lopinavir by comparing the peaks of the observed XRPD data of samples L-01, L-02, L-03, and L-04 with the polymorphic forms of lopinavir in the literature (Marques, 2017). We found out that the form of lopinavir obtained from methanol recrystallization (from now on referred to as L-met) fits the peaks of the samples L-01, L-02, and L-04, as seen in Fig. 3. The sample L-03, on the other hand, was revealed to be amorphous.

We performed Rietveld refinements using the software *TOPAS-Academic v6* (Coelho et al., 2011) and a quantitative phase analysis (QPA) (Bish and Howard, 1988) of all samples (for those comprised of more than one phase). Figs. S1 to S9 exhibit the refinements regarding the
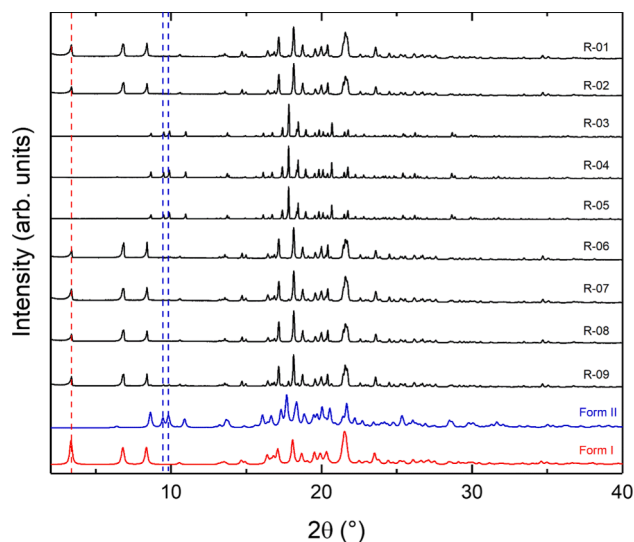

Fig. 2. X-ray powder diffractograms of the samples of R-01 to R-09 and the calculated powder patterns of Form I and Form II (obtained from the literature (Groom et al., 2016)) with normalized intensities. The red dashed line indicates the position of one characteristic peak of Form I, while the blue dashed lines indicate the position of two characteristic peaks of Form II. (For interpretation of the references to colour in this figure legend, the reader is referred to the web version of this article.)
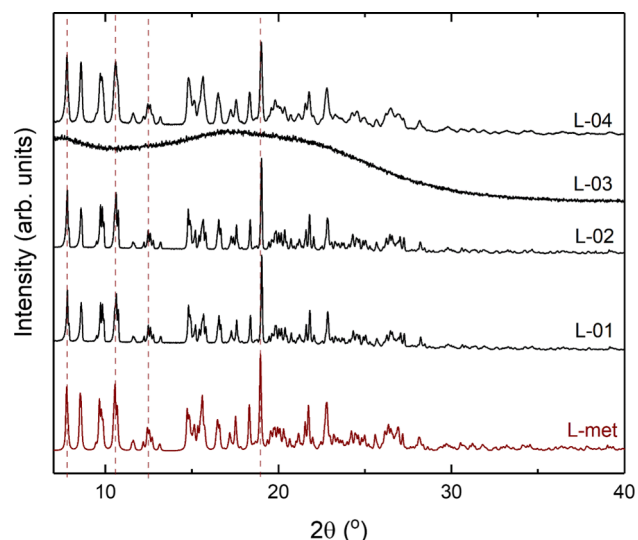

Fig. 3. X-ray powder diffractograms of the samples of lopinavir L-01 to L-04 and the calculated powder pattern for form L-met (Marques, 2017), with intensities normalized. The brown dashed lines indicate the characteristic peaks of the form L-met.

samples of R-01 to R-09. Figs. S10, S11, and S12 show the refinements of L-01, L-02, and L-04, respectively.

For clarity, the refinements are presented in a 2θ range from 2° to 60°. The mass fractions of each phase obtained from the refinements are displayed in Table 6.

Adopting a similar procedure to the one used to analyze the ritonavir and lopinavir diffractograms alone, we also performed a visual comparison of the samples described in Table 5, as shown in Fig. 4.

The comparison of the diffractograms of samples containing only R-06 before (shown in Fig. 2) and after the ball-milling process (R-06 (bm); Fig. 4) shows that the peaks remained in the same positions, and the peak intensities were only slightly reduced, suggesting that the polymorphic phase (Form I) remained unaltered, with partial amorphization taking place as evidenced by the increase in the baseline in the powder pattern. On the other hand, the physical mixtures of R-06 and L-03 – R-06 + L03 (bm) and R-06 + L-03 (hg) – exhibited peaks that coincide with some of those found in Form II. It suggests that the homogenization processes were responsible for a polymorphic phase transition, specifically from Form I to Form II, but only in the presence of L-03, suggesting that the miscibility between the two drugs impacts the polymorphic transformation.

The phase transition can be explained because Form II is a more stable polymorph than Form I, but more difficult to crystallize, according to Bauer et al. (Bauer et al., 2001). We can assume that the energy given by ball-milling or the hand-grinding processes might provide the activation energy for the transition of ritonavir into a more

Table 6
Mass fraction of each polymorph (Form I and Form II) in each one of the ritonavir samples.

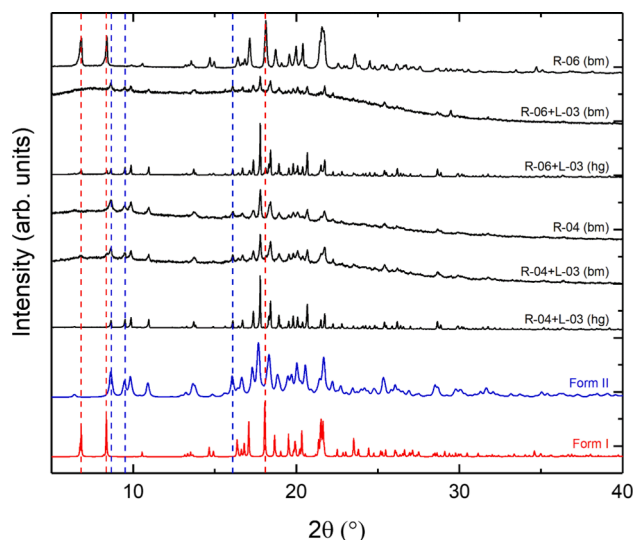|	Concentration (wt%)	
	Form I	Form II
R-01	3.0(3)	97.0(3)
R-02	56.1(4)	43.9(4)
R-03	0	100
R-04	0	100
R-05	0	100
R-06	100	0
R-07	96.7(3)	3.3(3)
R-08	100	0
R-09	87.5(4)	12.5(4)

Fig. 4. X-ray powder diffractograms of the samples shown in Table 5 and the calculated powder patterns for Form I and Form II (obtained from the literature (Groom et al., 2016)) with normalized intensities. The red dashed lines indicate two characteristic peaks of Form I, while the blue dashed lines indicate the position of two characteristic peaks of Form II of ritonavir. (For interpretation of the references to colour in this figure legend, the reader is referred to the web version of this article.)

stable form, but this is not sufficient for the transformation as the transition only happens on milling in the presence of L-03. The presence of the Form II peaks is more evident in the ball-milled sample, which is the more energetic milling process. The low-intensity peaks in the diffractogram of this sample also indicate an almost complete amorphization of R-06 (Form I) after ball-milling, but again, only in the presence of L-03. These results show that the presence of amorphous lopinavir significantly facilitates the transition of the ritonavir to its stable Form II, though the mechanism is not completely clear.

By performing the same comparison with the samples containing R-04, it was observed that the intensity of the peaks of the sample containing only R-04, as well as the one containing the physical mixture R-04 + L-03, both after ball-milling, exhibited a substantial reduction compared to the pristine R-04 sample. There was an increase in the powder pattern baseline, suggesting the ball milling resulted in a partial amorphization of the samples, regardless of the presence or not of L-03. On the other hand, hand-grinding of the R-04 + L03 (hg) mixture did not result in significant amorphization or other alterations (only a slight reduction in peak intensities) with respect to the sample containing only R-04 as received.

The Rietveld refinements of the samples shown in Table 5 are presented in Figs. S13 to S18, and the calculated concentrations of Forms I and II for each sample are summarized in Table 7. Due to the amorphous nature of samples L-03 and K1, we did not carry out Rietveld

Table 7
Mass fractions of each polymorph (Form I and Form II) in each one of the work samples.

	Concentration (wt%)	
	Form I	Form II
R-06	100	0
R-06 (bm)	100	0
R-06 + L-03 (bm)	8.70	91.30
R-06 + L-03 (hg)	26.73	73.27
R-04	0	100
R-04 (bm)	0	100
R-04 + L-03 (bm)	0	100
R-04 + L-03 (hg)	0	100

refinements. We have not quantified the amorphous fraction in the Rietveld refinements, only the proportions of the crystalline phases.

3.2. Optical microscopy imaging

By analyzing the optical microscopy images of ritonavir and comparing them with the crystal habits of those polymorphs described by Bauer et al. (Bauer et al., 2001), the most significant correlation found applied to the samples R-04, R-05, and R-06 in such a way that the two former ones exhibited a crystal habit compatible with the one of Form II (needles), whereas the latter exhibited a crystal habit similar to the one of Form I (rods). For those three samples, the results support the quantitative analysis initially performed. The microscope imaging of the samples R-04, R-05, and R-06 can be seen in Fig. 5(a), Fig. 5(b), and Fig. 5(c), respectively.

3.3. Differential scanning calorimetry

The DSC curves for the samples displayed in Table 7 are shown in Fig. 6, Fig. S19, Fig. S20, and Fig. S21.

The DSC curves show that the milling process resulted in a partial amorphization for both ritonavir polymorphs, as denoted by the presence of the glass transition temperature (T_g), resulting in different thermal properties; this fact was also noticed in the X-ray patterns. In the case of R-06 (bm), a T_g was observed at 77 °C (Fig. S19), which is higher than the one reported by Zhou et al. (Zhou et al., 2007) at 50 °C; this could be assigned to the effect of the thermal history of the samples (Kato et al., 2001) since the preparation procedures were different. Despite a certain degree of amorphization, the main melting event was maintained in the same temperature range as the reported Form I, indicating no significant polymorphic changes (Fig. 6a and Fig. 6b). However, the first derivative in the DSC (Fig. S19) curve reveals an additional small event observed in the range of 110–115 °C that may be assigned to a possible presence of Form IV, as discussed below.

The DSC curve of sample R-04 (bm) presents a superposed glass transition of the amorphous fraction with subsequent recrystallization in the temperature range of 50 to 70 °C, followed by the melting at $T_{onset} =$ 94 °C (Fig. S20). However, the melting enthalpy ($\Delta H_m = 69$ J g^{-1}) was significantly lower than that reported by Chemburkar and collaborators (Chemburkar et al., 2000) (values reported: $\Delta H_m = 87.8$ J g^{-1}), while the melting temperature was the same ($T_{melting} = 125$ °C). This observed decrease in the melting enthalpy can be related to the properties of the crystal Form IV reported by Morissette and colleagues (Morissette et al., 2003) (values reported: $\Delta H_m = 60.8$ J g^{-1}; $T_{melting} = 116$ °C). Consequently, the results may suggest that the amorphous fraction obtained from Form II recrystallizes to Form IV. This possibility is reinforced by Kawakami (Kawakami, 2015), who demonstrated that quenched glasses of ritonavir crystallize to Form IV, followed by transformation to Form I after one week.

On the other hand, an amorphous contribution generated from the unstable Form I converted directly into the same form. Furthermore, R-04 (bm) crystallization temperature starts around 52 °C (Fig. S20), suggesting that T_g is lower than this value. This lower T_g and differences in the surface area decrease the energetic barrier for nucleation and can facilitate recrystallization, which is a plausible explanation for the observed differences between the two samples (Kawakami, 2015).

The DSC curves of the sample L-03 showed endothermic events in the temperature range of 60 °C to 70 °C (Fig. 6 c,d, and Fig. S21), which are characteristic of endothermic relaxation related to amorphous materials and consonant with the powder diffraction results. Also, this region is congruent with the T_g of lopinavir (74.5 °C) reported by Lemmer and Liebenberg (Lemmer and Liebenberg, 2013).

In general, the mixtures between ritonavir and lopinavir presented a similar behavior. After this lopinavir thermal transition, ritonavir peaks are totally or partially suppressed, which indicates the solubilization of ritonavir in the melted lopinavir, revealing a certain degree of
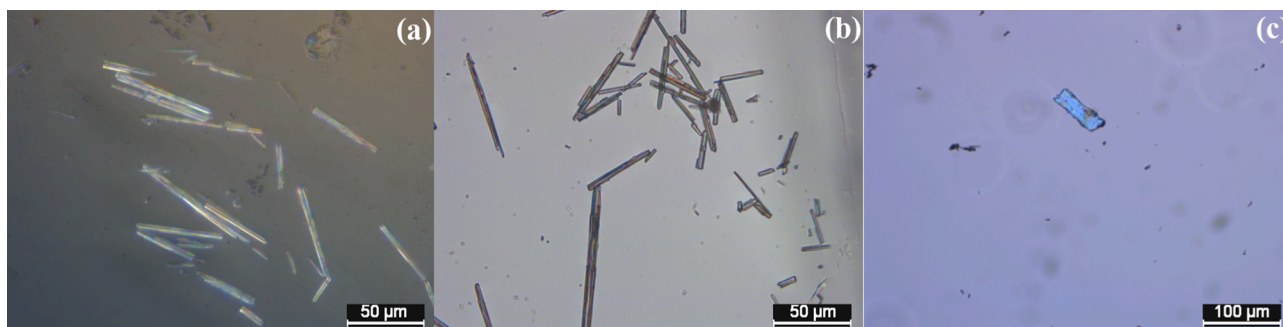
Fig. 5. Optical microscopy images of the samples (a) R-04, (b) R-05, and (c) R-06 of ritonavir.
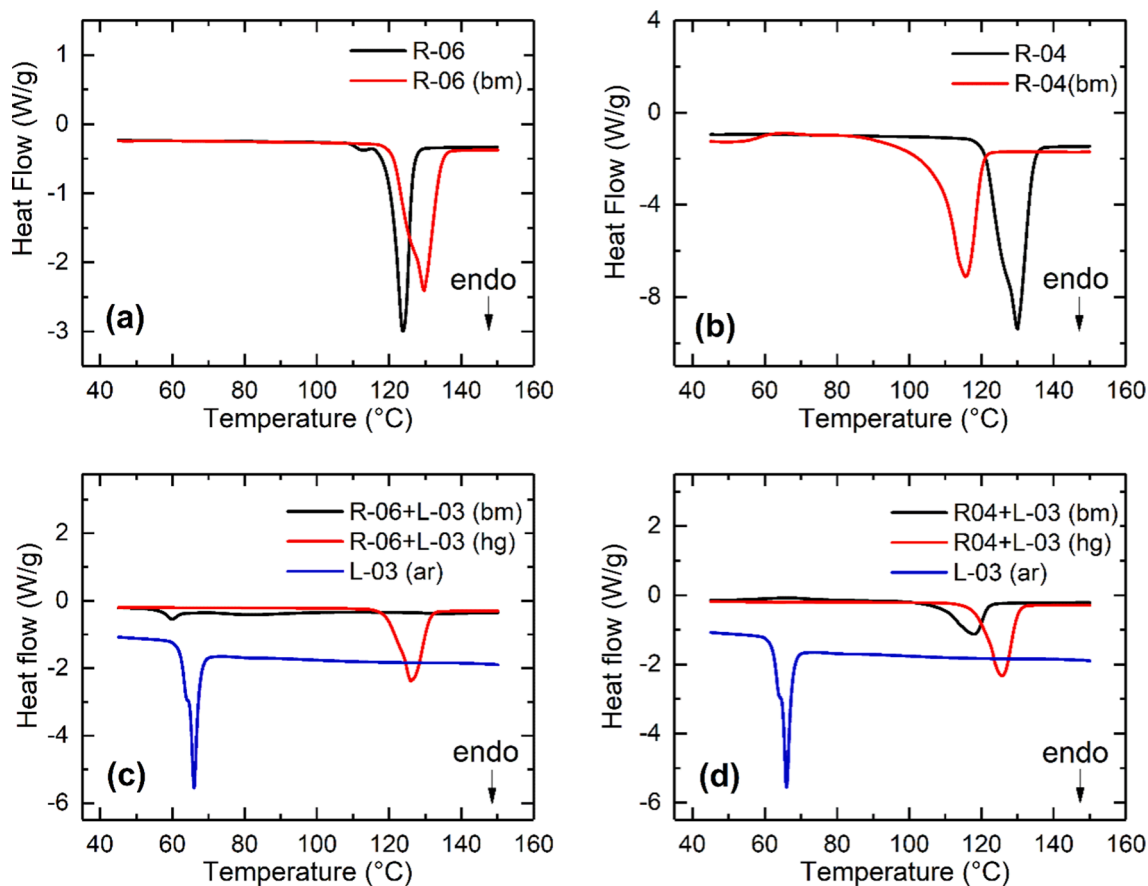

Fig. 6. Comparison among the DSC curves of the samples: (a) R-06 and R-06 (bm), (b) R-04 and R-04 (bm), (c) R-06 + L-03 (bm), R-06 + L-03 (hg) and L-03 and (d) R-04 + L-03 (bm), R-04 + L-03 (hg) and L-03.

miscibility between the drugs, which agrees with previous reports from Trasi and Taylor (Trasi and Taylor, 2015a, 2015b).

3.4. Pair distribution function

The X-ray pair distribution functions (PDF) for the ball-milled L-03, R-04, R-06, and R-04+L-03, R-06 + L-03 were measured and shown in Fig. 7(a).

The long-range order appears as the signal in the high-r region of the PDFs. Fig. 7(a) shows that the L-03 sample is amorphous (has no signal beyond 10 Å); similar behaviors have also been observed in amorphous drug-polymer dispersion (Bezzon et al., 2021; Terban et al., 2022). This signal range is slightly smaller than the size of a single lopinavir molecule, indicating that the spatial distribution of molecules is fairly random and that the molecule itself has some flexibility. In comparison,

the R-04 and R-06 PDFs indicate that the samples have an ordered structure over a broader range. The differences in the crystal structures of R-04 and R-06 can be identified from the different signals of the respective PDFs in the high-r region. There is no significant enhancement in long-range order after milling the R-04 + L-03 mixture or the R-06 + L-03 one.

To reveal the conformation of the molecules in the L-03, R-04, and R-06, a discrete molecule structure model is used to fit the data. The PDF is calculated according to.

$$G(r) = \frac{2}{\pi} \int_{Q_{min}}^{Q_{max}} Q(S(Q) - 1)\sin(Qr)dQ, \tag{1}$$

$$S(Q) = \frac{I(Q)}{N\overline{f}^2} + \frac{\overline{f^2} - \overline{f}^2}{\overline{f}^2} \tag{2}$$

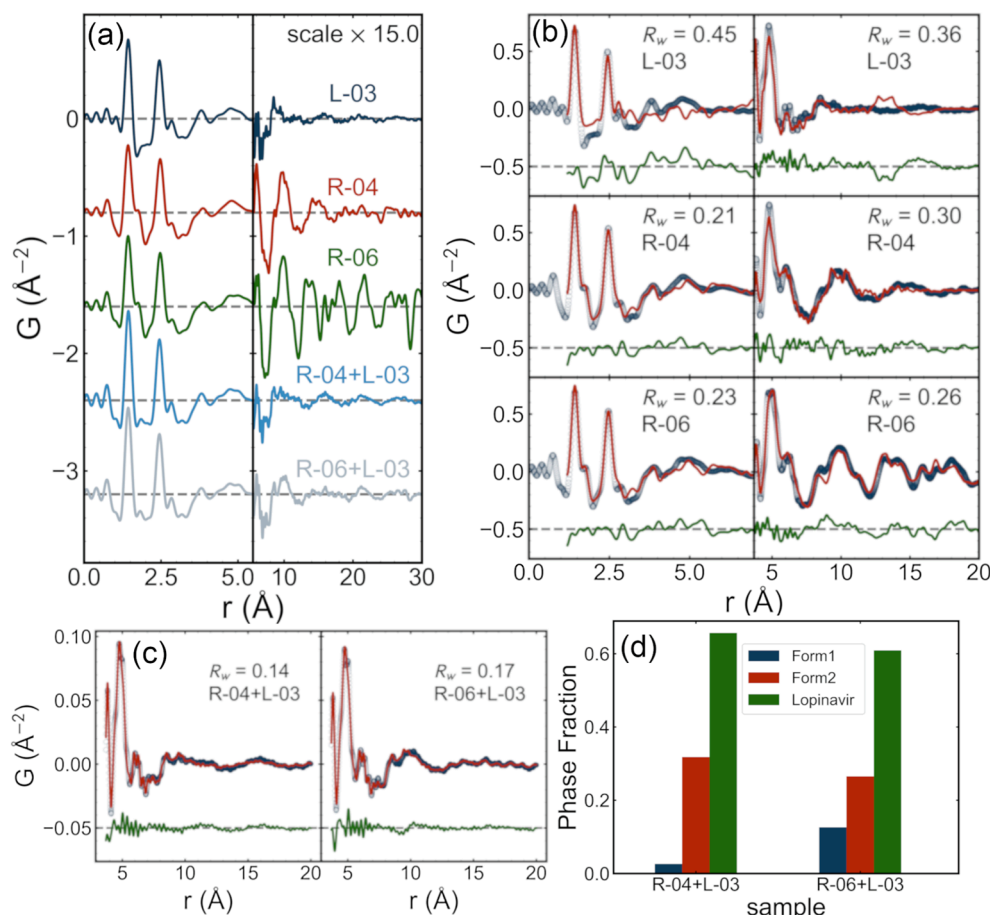**Fig. 7.** (a) The PDFs of L-03, R-04, R-06, R-04 + L-03 and R-06 + L-03. The left panel shows the data in 0 Å $\leq$ r $\leq$ 5.5 Å and the right panel shows the data in 5.5 Å $\leq$ r $\leq$ 30 Å. The data in the right panel is scaled by a multiplier for better visualization. (b) The fits of L-03, R-04, and R-06 data using the molecule models in 1.2 Å $\leq$ r $\leq$ 7.0 Å and the crystal models in 3.7 Å $\leq$ r $\leq$ 20.0 Å. The blue circles are the PDF data points, the red curves are the calculated PDF, and the green curves are residuals. (c) The fits of R-04 + L-03 and R-06 + L-03 in 3.7 Å $\leq$ r $\leq$ 20.0 Å. (d) The phase fraction of amorphous lopinavir, nanocrystalline ritonavir Form I, and nanocrystalline ritonavir Form II. (For interpretation of the references to colour in this figure legend, the reader is referred to the web version of this article.)

$$I(Q) = \sum_{i \neq j} f_i f_j \frac{\sin(Qr_{ij})}{Qr_{ij}}, \qquad (3)$$

where Q is the momentum transfer and $S(Q)$ is the structure factor defined as the normalized intensity of coherent scattering shown in Eq. (2) and Eq. (3) (Billinge, 2008). The f is the form factor, i, j are the indexes of the atoms, and r_{ij} is the distance between the ith and jth atom. Here, the r_{ij} is calculated using the positions of atoms in a single molecule. The refined parameters are shown in Table S1. We use the value of R_w and the residual curve to test whether the conformation is the same as reported in the crystal structure database (Céolin and Rietveld, 2015; Marques, 2017). The results of the fits are shown in Fig. 7(b). For R-04 and R-06, the R_w is small, and the residuals are close to zero; thus, the local conformation of the ritonavir molecule is well described by that in the known crystal structures of ritonavir Form II and Form I for R-04 and R-06, respectively. For L-03, the R_w is relatively large, and there are non-trivial features in the residual curve. It indicates that the conformation of molecules in the L-03 sample differs from the one reported for the L-03 crystal structure (Céolin and Rietveld, 2015; Marques, 2017).

An attenuated crystal model is used to fit the data to understand the crystal structures in the L-03, R-04, and R-06 samples. The PDF is calculated according to Eq. (4) and Eq. (5),

$$G(r) = \gamma(r)\left(\frac{R(r)}{r} - 4\pi r \rho_0\right), \qquad (4)$$

$$R(r) = \frac{1}{N}\sum_{i \neq j}\frac{f_i f_j}{\overline{f}^2}\phi(r - r_{ij}), \qquad (5)$$

where $\gamma(r)$ is the characteristic function for spherical crystallites, ρ_0 is

the average number density of the crystal, f is the form factor at $Q = 0$, ϕ is the Gaussian function, and r_{ij} is the distance between the ith and jth atom in the crystal structure. The fits are shown in Fig. 7(b). The fit of lopinavir is not good beyond 10 Å, which is expected since the sample is disordered. The ritonavir PDFs are well fit by the relevant attenuated crystal models. The results confirm that the nanocrystalline structure of R-04 is locally Form II, and that of R-06 is Form I. The parameters of the fits are reproduced in Table S2.

We now turn to the co-ground L + R mixture samples to analyze which phases are inside the R-04 + L-03 and R-06 + L-03 mixtures after grinding. A multiphase model is proposed in Eq. (6),

$$G_{mix} = x_L G_L + x_{R1} G_{R1} + x_{R2} G_{R2} + \epsilon, \qquad (6)$$

where the G_{mix} is the PDF of the mixture, G_L is the PDF of the amorphous lopinavir phase, represented by the PDF data of L-03, G_{R1} is the nano-crystal ritonavir Form I, represented by the PDF data of R-06, G_{R2} is the nanocrystal ritonavir Form II, represented by the PDF data of R-04, $x_i (i = L, R1, R2)$ are the scales of each PDF, and ϵ is the error term, assumed as white noise.

Fig. 7(d) shows that the model fits well with the R-04 + L-03 and R-06 + L-03 data. The phase fractions obtained from the fit are plotted in Fig. 7(d). Interestingly, there is more Form II ritonavir in the R-06 + L-03 mixture despite the starting material before grinding being R-06 in Form I, as seen directly in the powder diffraction measurements in Table 7. It suggests that a proportion of ritonavir Form I transformed into Form II after ball milling with lopinavir. This is consistent with the results from XRD in Table 7. The major phase is still Form II in the R-04 + L-03 mixture, unchanged from the starting phase, R-04. It indicates that the ritonavir Form I nanocrystals transform into Form II if milled with lopinavir, while the ritonavir Form II nanocrystals will keep the same

form after the milling with lopinavir. The PDF fits indicate that the samples are still predominantly amorphous lopinavir with around 20 wt % of ritonavir, predominantly in Form II, even when it started in Form I before grinding. There is no evidence of amorphous ritonavir even after grinding.

4. Conclusion

Rietveld refinement and PDF analysis were used to evaluate the polymorphic composition of different ritonavir batches and manufacturing sources, highlighting significant variations in phase purity that could have consequences for the processing, and solid-state properties, representing risks for product quality. One out of four batches of lopinavir was completely amorphous, while the other three displayed similar X-ray patterns. DSC analysis revealed miscibility between the already amorphous lopinavir sample and the crystalline ritonavir ones and that different and unexpected crystalline forms of ritonavir, as well as some amorphous components, were produced. This general trend was supported by the PDF results, which also showed variations in the lopinavir molecule conformation in the disordered state from that in the crystalline state. It was possible to quantify the phases, including the amorphous component from the PDF model fits. A surprising discovery was that generation of ritonavir Form II on milling in the presence of lopinavir, but not when milling pure ritonavir under the same conditions.

These findings suggest that more investigation on ritonavir and lopinavir combinations is necessary to fully elucidate the individual contribution and solid-state interactions of those essential anti-HIV drugs, especially in tests against COVID-19.

CRediT authorship contribution statement

Lucas Barboza Moreira Pinheiro: Conceptualization, Methodology, Formal analysis, Writing – original draft. **Songsheng Tao:** Data curation, Writing – review & editing, Software. **Elizabeth Culbertson:** Data curation. **Gabriel Lima Barros de Araujo:** Formal analysis, Writing – review & editing. **Simon J.L. Billinge:** Formal analysis, Writing – review & editing, Software. **Fabio Furlan Ferreira:** Methodology, Resources, Formal analysis, Writing – original draft, Visualization, Funding acquisition, Project administration, Supervision.

Declaration of Competing Interest

The authors declare that they have no known competing financial interests or personal relationships that could have appeared to influence the work reported in this paper.

Data availability

Data will be made available on request.

Acknowledgments

Appendix A. Supplementary material

Supplementary data to this article can be found online at https://doi.org/10.1016/j.ijpharm.2022.122329.

References

Ataollahi, N., Broseghini, M., Ferreira, F.F., Susana, A., Pizzato, M., Scardi, P., 2021. Effect of High-Energy Milling on the Dissolution of Anti-HIV Drug Efavirenz in Different Solvents. ACS Omega 6, 12647–12659. https://doi.org/10.1021/acsomega.1c00712.

Bauer, J., Spanton, S., Henry, R., Quick, J., Dziki, W., Porter, W., Morris, J., 2001. Ritonavir: An Extraordinary Case of Conformational Polymorphism. Pharm. Res. 18, 859–866.

Bezzon, V.D.N., Ferreira, F.F., Smith, P., Benmore, C.J., Byrn, S.R., de Araujo, G.L.B., 2021. Amorphous dispersions of flubendazole in hydroxypropyl methylcellulose: Formulation stability assisted by pair distribution function analysis. Int. J. Pharm. 600, 120500 https://doi.org/10.1016/j.ijpharm.2021.120500.

Bezzon, V.D.N., Pinto, R.d.S., de Araújo, G.L.B., de Lima, J.C., Ferreira, F.F., 2022. Describing the Influence of Ball-milling on the Amorphization of Flubendazole Using the PDF and RMC Methods with X-ray Powder Diffraction Data. J. Pharm. Sci. 111 (11), 3054–3063.

Billinge, S., 2008. Chapter 16. Local Structure from Total Scattering and Atomic Pair Distribution Function (PDF) Analysis. In: Powder Diffraction. Royal Society of Chemistry, Cambridge, pp. 464–493. https://doi.org/10.1039/9781847558237-00464.

Bish, D.L., Howard, S.A., 1988. Quantitative phase analysis using the Rietveld method. J. Appl. Crystallogr. 21, 86–91. https://doi.org/10.1107/S0021889887009415.

Bruno, I.J., Cole, J.C., Edgington, P.R., Kessler, M., Macrae, C.F., McCabe, P., Pearson, J., Taylor, R., 2002. New software for searching the Cambridge Structural Database and visualizing crystal structures. Acta Crystallogr. Sect. B Struct. Sci. 58, 389–397. https://doi.org/10.1107/S0108768102003324.

Céolin, R., Rietveld, I.B., 2015. The topological pressure-temperature phase diagram of ritonavir, an extraordinary case of crystalline dimorphism. Ann. Pharm. Françaises 73, 22–30. https://doi.org/10.1016/j.pharma.2014.09.003.

Chandwani, A., Shuter, J., 2008. Lopinavir/ritonavir in the treatment of HIV-1 infection: a review. Ther. Clin. Risk Manag. 4, 1023–1033. https://doi.org/10.2147/tcrm.s3285.

Chemburkar, S.R., Bauer, J., Deming, K., Spiwek, H., Patel, K., Morris, J., Henry, R., Spanton, S., Dziki, W., Porter, W., Quick, J., Bauer, P., Donaubauer, J., Narayanan, B.A., Soldani, M., Riley, D., McFarland, K., 2000. Dealing with the Impact of Ritonavir Polymorphs on the Late Stages of Bulk Drug Process Development. Org. Process Res. Dev. 4, 413–417. https://doi.org/10.1021/op000023y.

Chupas, P.J., Qiu, X., Hanson, J.C., Lee, P.L., Grey, C.P., Billinge, S.J.L., 2003. Rapid-acquisition pair distribution function (RA-PDF) analysis. J. Appl. Crystallogr. 36, 1342–1347. https://doi.org/10.1107/S0021889803017564.

Coelho, A.A., Evans, J., Evans, I., Kern, A., Parsons, S., 2011. The TOPAS symbolic computation system. Powder Diffr. 26, S22–S25. https://doi.org/10.1154/1.3661087.

Descamps, M., Willart, J.F., Dudognon, E., Caron, V., 2007. Transformation of Pharmaceutical Compounds upon Milling and Comilling: The Role of Tg. J. Pharm. Sci. 96, 1398–1407. https://doi.org/10.1002/jps.20939.

Douek, D.C., Roederer, M., Koup, R.A., 2009. Emerging Concepts in the Immunopathogenesis of AIDS. Annu. Rev. Med. 60, 471–484. https://doi.org/10.1146/annurev.med.60.041807.123549.

Erizal, Z., Cahyati, S.Y., Nurono, S.S., Halim, A., 2008. Effect of Milling on Solid State Transformation of Sulfamethoxazole. Int. J. Pharmacol. 4, 140–144. https://doi.org/10.3923/ijp.2008.140.144.

Groom, C.R., Bruno, I.J., Lightfoot, M.P., Ward, S.C., 2016. The Cambridge Structural Database. Acta Crystallogr. Sect. B Struct. Sci. Cryst. Eng. Mater. 72, 171–179. https://doi.org/10.1107/S2052520616003954.

Gurunath, S., Pradeep Kumar, S., Basavaraj, N.K., Patil, P.A., 2013. Amorphous solid dispersion method for improving oral bioavailability of poorly water-soluble drugs. J. Pharm. Res. 6, 476–480. https://doi.org/10.1016/j.jopr.2013.04.008.

Hameed, G.S., 2019. Controlling phase transformation during milling in the pre-formulation of Active pharmaceutical Ingredients. Al Mustansiriyah J. Pharm. Sci. 19, 37–46. https://doi.org/10.32947/ajps.19.02.0402.

Juhás, P., Davis, T., Farrow, C.L., Billinge, S.J.L., 2013. PDFgetX3: a rapid and highly automatable program for processing powder diffraction data into total scattering pair distribution functions. J. Appl. Crystallogr. 46, 560–566. https://doi.org/10.1107/S0021889813005190.

Kato, Y., Hagiwara, T., Suzuki, T., Takai, R., 2001. The Effect of Thermal History on The Glass Transition of Dried Gelatin Gel. Trans. Mater. Res. Soc. Japan 26, 659–662.

Kawakami, K., 2015. Surface Effects on the Crystallization of Ritonavir Glass. J. Pharm. Sci. 104, 276–279. https://doi.org/10.1002/jps.24229.

Klein, C.E., Chiu, Y.-L., Awni, W., Zhu, T., Heuser, R.S., Doan, T., Breitenbach, J., Morris, J.B., Brun, S.C., Hanna, G.J., 2007. The Tablet Formulation of Lopinavir/Ritonavir Provides Similar Bioavailability to the Soft-Gelatin Capsule Formulation With Less Pharmacokinetic Variability and Diminished Food Effect. JAIDS J. Acquir. Immune Defic. Syndr. 44, 401–410. https://doi.org/10.1097/QAI.0b013e31803133c5.

Kupferschmidt, K., Cohen, J., 2020. Race to find COVID-19 treatments accelerates. Science (80-.) 367, 1412–1413. https://doi.org/10.1126/science.367.6485.1412.

Lemmer, H.J.R., Liebenberg, W., 2013. Preparation and evaluation of metastable solid-state forms of lopinavir. Pharmazie 68, 327–332.

Leuner, C., 2000. Improving drug solubility for oral delivery using solid dispersions. Eur. J. Pharm. Biopharm. 50, 47–60. https://doi.org/10.1016/S0939-6411(00)00076-X.

Marques, A.C.S., 2017. Estudo cristalográfico de formas sólidas do antirretroviral lopinavir. Universidade Federal Fluminense.

Morissette, S.L., Soukasene, S., Levinson, D., Cima, M.J., Almarsson, O., 2003. Elucidation of crystal form diversity of the HIV protease inhibitor ritonavir by high-throughput crystallization. Proc. Natl. Acad. Sci. 100, 2180–2184. https://doi.org/10.1073/pnas.0437744100.

Najjar-Debbiny, R., Gronich, N., Weber, G., Khoury, J., Amar, M., Stein, N., Goldstein, L. H., Saliba, W., 2022. Effectiveness of Paxlovid in Reducing Severe Coronavirus Disease 2019 and Mortality in High-Risk Patients. Clin. Infect. Dis. ciac443. https://doi.org/10.1093/cid/ciac443.

Parthasaradhi Reddy, B., Rathnakar Reddy, K., Raji Reddy, R., Muralidhara Reddy, D., Subash Chander Reddy, K., 2013. Polymorphs of lopinavir. US8445506.

Parthasaradhi Reddy, B., Rathnakar Reddy, K., Raji Reddy, R., Muralidhara Reddy, D., Subash Chander Reddy, K., 2014. Novel polymorphs of lopinavir. EP2393786 B1.

Prather, K.A., Wang, C.C., Schooley, R.T., 2020. Reducing transmission of SARS-CoV-2. Science (80-.) 368, 1422–1424. https://doi.org/10.1126/science.abc6197.

Terban, M.W., Madhau, L., Cruz-Cabeza, A.J., Okeyo, P.O., Etter, M., Schulz, A., Rantanen, J., Dinnebier, R.E., Billinge, S.J.L., Moneghini, M., Hasa, D., 2022. Controlling desolvation through polymer-assisted grinding. CrystEngComm 24 (12), 2305–2313.

Trasi, N.S., Taylor, L.S., 2015a. Thermodynamics of Highly Supersaturated Aqueous Solutions of Poorly Water-Soluble Drugs—Impact of a Second Drug on the Solution Phase Behavior and Implications for Combination Products. J. Pharm. Sci. 104, 2583–2593. https://doi.org/10.1002/jps.24528.

Trasi, N.S., Taylor, L.S., 2015b. Dissolution performance of binary amorphous drug combinations—Impact of a second drug on the maximum achievable supersaturation. Int. J. Pharm. 496, 282–290. https://doi.org/10.1016/j.ijpharm.2015.10.026.

Trask, A.V., Shan, N., Motherwell, W.D.S., Jones, W., Feng, S., Tan, R.B.H., Carpenter, K. J., 2005. Selective polymorph transformation via solvent-drop grinding. Chem. Commun. (7), 880.

UNAIDS, n.d. Fact Sheet - July 2021 [WWW Document]. URL https://www.unaids.org/en/resources/fact-sheet.

Yang, X., Juhas, P., Farrow, C.L., Billinge, S.J.L., 2014. xPDFsuite: an end-to-end software solution for high throughput pair distribution function transformation, visualization and analysis.

Zhou, D., Grant, D.J.W., Zhang, G.G.Z., Law, D., Schmitt, E.A., 2007. A Calorimetric Investigation of Thermodynamic andMolecular Mobility Contributions to the Physical Stability of Two Pharmaceutical Glasses. J. Pharm. Sci. 96, 71–83. https://doi.org/10.1002/jps.20633.